Published OnlineFirst June 1, 2010; DOI: 10.1158/1535-7163.MCT-09-1134

Research Article

Molecular Cancer Therapeutics

A Human Monoclonal Antibody against Insulin-Like Growth Factor-II Blocks the Growth of Human Hepatocellular Carcinoma Cell Lines *In vitro* and *In vivo*

Daniel T. Dransfield[1], Edward H. Cohen[1], Qing Chang[1], Lindsay G. Sparrow[2], John D. Bentley[2], Olan Dolezal[2], Xiaowen Xiao[2], Thomas S. Peat[2], Janet Newman[2], Patricia A. Pilling[2], Tram Phan[2], Ilka Priebe[3], Gemma V. Brierley[3], Niksa Kastrapeli[1], Kris Kopacz[1], Diana Martik[1], Dina Wassaf[1], Douglas Rank[1], Greg Conley[1], Yan Huang[1], Timothy E. Adams[2], and Leah Cosgrove[3]

Abstract

Elevated expression of insulin-like growth factor-II (IGF-II) is frequently observed in a variety of human malignancies, including breast, colon, and liver cancer. As IGF-II can deliver a mitogenic signal through both IGF-IR and an alternately spliced form of the insulin receptor (IR-A), neutralizing the biological activity of this growth factor directly is a potential alternative option to IGF-IR–directed agents. Using a Fab-displaying phage library and a biotinylated precursor form of IGF-II (1–104 amino acids) as a target, we isolated Fabs specific for the E-domain COOH-terminal extension form of IGF-II and for mature IGF-II. One of these Fabs that bound to both forms of IGF-II was reformatted into a full-length IgG, expressed, purified, and subjected to further analysis. This antibody (DX-2647) displayed a very high affinity for IGF-II/IGF-IIE (K_D value of 49 and 10 pmol/L, respectively) compared with IGF-I (~10 nmol/L) and blocked binding of IGF-II to IGF-IR, IR-A, a panel of insulin-like growth factor–binding proteins, and the mannose-6-phosphate receptor. A crystal complex of the parental Fab of DX-2647 bound to IGF-II was resolved to 2.2 Å. DX-2647 inhibited IGF-II and, to a lesser extent, IGF-I–induced receptor tyrosine phosphorylation, cellular proliferation, and both anchorage-dependent and anchorage-independent colony formation in various cell lines. In addition, DX-2647 slowed tumor progression in the Hep3B xenograft model, causing decreased tumoral CD31 staining as well as reduced IGF-IIE and IGF-IR phosphorylation levels. Therefore, DX-2647 offers an alternative approach to targeting IGF-IR, blocking IGF-II signaling through both IGF-IR and IR-A. *Mol Cancer Ther; 9(6); 1809–19. ©2010 AACR.*

Introduction

Hepatocellular carcinomas (HCC) account for the majority of primary liver cancers, ranking third as a cause of cancer mortality (1). The major etiologic factors are well established and include viral hepatitis (B and C), primary liver disease with hereditary origins (e.g., hemochromatosis), alcohol use, and mycotoxin exposure. Therapeutic intervention is dictated by the stage of the disease at diagnosis and may include tumor resection and liver transplantation, percutaneous and transarterial intervention, radiation, and other therapies. For advanced HCC, no standard therapy exists, although a phase III clinical trial of the multikinase inhibitor sorafenib did result in significantly improved survival (2).

There is compelling clinical and experimental evidence that insulin-like growth factor-II (IGF-II) plays a key role in the pathogenesis of HCC (3). IGF-II is a maternally imprinted embryonic growth factor that can elicit a spectrum of cellular responses, including proliferation and protection from apoptosis, through activation of IGF-IR, an alternatively spliced form of the insulin receptor (IR-A), and the mannose-6-phosphate receptor (IGF-IIR; ref. 4). The mature form of IGF-II (67 amino acids) arises following posttranslational processing, including *O*-glycosylation and endoproteolysis, of a pro-IGF-II precursor (5). Elevated expression of IGF-II, in part the result of loss of imprinting, is observed in a variety of human malignancies, including cancers of the breast, colon, and liver (reviewed in ref. 4). This may be accompanied by the secretion of aberrantly processed pro-IGF-II isoforms with novel properties by some tumor types). With respect to HCC, the reactivation of *Igf-II* transcription from fetal-specific promoter elements is observed in

Authors' Affiliations: [1]Dyax Corp., Cambridge, Massachusetts; [2]CSIRO Molecular and Health Technologies, Parkville, Victoria, Australia; and [3]CSIRO Molecular and Health Technologies, Adelaide, South Australia, Australia

Note: Supplementary material for this article is available at Molecular Cancer Therapeutics Online (http://mct.aacrjournals.org/).

The crystal structure has been deposited in the Protein Data Bank with accession code 3KR3.

Corresponding Author: Daniel T. Dransfield, Discovery Research, Dyax Corp., 8th Floor, 300 Technology Square, Cambridge, MA 02139. Phone: 617-250-5729; Fax: 617-225-2501. E-mail: ddransfield@dyax.com

doi: 10.1158/1535-7163.MCT-09-1134

Published OnlineFirst June 1, 2010; DOI: 10.1158/1535-7163.MCT-09-1134

>40% of primary HCC specimens analyzed (8, 9), with a 40- to 100-fold increase in IGF-II mRNA in 25% of tumor samples relative to normal adult liver (10). Immunohistochemical detection of IGF-II peptide was found in all HCC tissue samples screened (11), whereas IGF-II mRNA in peripheral blood mononuclear cells has been detected in 100% of patients with HCC and extrahepatic metastasis (12). Hepatic expression of an *Igf-II* transgene gives rise to HCC in mice after a long latency (13). The reexpression of fetal IGF-II mRNAs during hepatocarcinogenesis in a number of independent transgenic mouse models strongly supports a role for IGF-II in multistep liver carcinogenesis (14, 15).

The key role played by the IGF axis in the establishment and maintenance of cellular transformation has focused on IGF-IR as a therapeutic target (16). The receptor, a heterotetrameric transmembrane tyrosine kinase, binds both IGF-II and the related growth factor, IGF-I, with high affinity; germline inactivation of the *Igf-Ir* gene renders murine fibroblasts resistant to transformation by a number of viral and cellular oncogenes (17, 18). To date, there are >25 therapeutic candidates, predominantly small-molecule tyrosine kinase inhibitors and monoclonal antibodies, targeting IGF-IR that are at various stages of development (19). Less attention has been paid to neutralizing the ligands themselves, perhaps in part due to the complex biology that underpins their bioavailability. Although the serum levels of IGF-I and IGF-II in adults are quite high (e.g., mean values of 248 and 929 ng/mL, respectively; ref. 20), >90% of both growth factors are found complexed with members of a family of six insulin-like growth factor–binding proteins (IGFBP), predominantly IGFBP-3 complexed to the acid labile subunit (reviewed in ref. 21). The circulating levels of these complexes have obvious implications for the pharmacokinetic properties of any ligand-neutralizing entity. Nonetheless, neutralizing the biological activity of IGF-II directly is an attractive therapeutic option in light of the ability of IGF-II to bind/activate not only IGF-IR but also IR-A, the aberrant expression of which is found in a number of human malignancies (reviewed in ref. 22).

Along these lines, i.p. administration of a mouse monoclonal cross-reactive to human IGF-I and IGF-II suppressed the development of new bone tumors and the progression of established tumors (23). The same antibody inhibited tumor growth and prolonged survival in a mouse model of hepatic metastasis (24). Human monoclonal antibodies have been isolated that bind IGF-II and block the growth/migration of a number of human tumor lines *in vitro* (25) and, as was recently described, block growth of prostate cancer cells in a human bone environment (26). In the present study, we describe the isolation and characterization of a phage-derived human monoclonal antibody with high affinity against IGF-II and report on the *in vitro* and *in vivo* efficacy of this antibody.

Materials and Methods

Cell culture

All cell culture media and supplements were obtained from Mediatech, Inc. Ba/F3 cells were purchased from the German Resource Centre for Biological Material cultured in RPMI 1640 supplemented with 10% heat-inactivated fetal bovine serum (FBS), 10 ng/mL interleukin (IL)-3 (R&D Systems), 100 IU/mL penicillin, and 100 μg/mL streptomycin. All remaining cell lines were purchased from the American Type Culture Collection. HepG2 and Hep3B were cultured in MEM supplemented with 10% heat-inactivated FBS, 100 IU/mL penicillin, and 100 μg/mL streptomycin. Colo205 cells were cultured in RPMI 1640 supplemented with 10% heat-inactivated FBS, 100 IU/mL penicillin, and 100 μg/mL streptomycin. R-IR-A (27) and R-IGF-IR cells (a gift from Dr. E. Bonython, University of Adelaide) were cultured in DMEM supplemented with 10% heat-inactivated FCS and 0.05% geneticin. All cell lines were maintained in a 37°C incubator with 5% CO_2.

Ba/F3 proliferation assay

Ba/F3 cells are an IL-3–dependent murine pro-B-cell line established from peripheral blood derived from a BALB/c mouse in which IL-4 synergizes with IGF-I in stimulating proliferation in an IL-3–independent manner (28). Ba/F3 cells were seeded into 96-well plates (5×10^4 per well) in IL-3–free medium. IGF-II (100 ng/mL; R&D Systems) or IGF-IIE (200 ng/mL; Novozymes GroPep) and IL-4 (50 ng/mL) at final concentrations were added. DX-2647 at the indicated concentrations was added, and the cells were cultured for an additional 2 days at 37°C and 5% CO_2. The total number of cells was determined using the MTS assay kit (CellTiter 96 Aqueous One Solution Reagent, Promega).

Surface plasmon resonance analysis

Surface plasmon resonance (SPR) measurements were done using a Biacore 3000. Goat anti-human Fc fragment–specific IgG (Jackson ImmunoResearch Laboratories) was immobilized by amine coupling on a CM5 sensor chip at ~5,000 relative units, and DX-2647 was captured on the derivatized flow cell by injecting a 20 nmol/L solution of antibody for 1 minute at 5 μL/min. To measure the kinetic parameters of DX-2647 interaction with IGF ligand, 2-fold serial dilutions prepared from 125, 50, and 25 nmol/L solutions of IGF-I (R&D Systems), IGF-II, and IGF-IIE, respectively, were injected in duplicate for 5 minutes at 50 μL/min, with a 10-minute dissociation phase. IGF-related proteins were injected at 500 nmol/L to assess potential cross-reactivity. For competition studies, IGF-II or IGF-IIE at 50 nmol/L was preincubated with each receptor or IGFBP at 500 nmol/L before injection over captured DX-2647. The sensor chip surface was regenerated with a 30-second pulse of 10 mmol/L glycine (pH 1.5) at a flow rate of 100 μL/min. Measurements were done at 25°C using HBS-P [10 mmol/L HEPES (pH 7.4), 150 mmol/L

Published OnlineFirst June 1, 2010; DOI: 10.1158/1535-7163.MCT-09-1134

NaCl, and 0.005% surfactant P20] as the running buffer. The reference flow cell was activated and blocked in a mock amine coupling reaction. Data were double referenced and fit to a 1:1 binding model using BIAevalution v.4.1 software.

Crystallization and structure analysis

Crystallization was done as previously reported (29). In brief, the crystals were grown using the sitting drop vapor diffusion technique at 293°K with reservoir conditions of 118 mmol/L $CaCl_2$, 18.5% (w/v) PEG 6000, and 10% (v/v) propionate-cacodylate-Bis-Tris propane buffer (pH 5.3; ref. 30). The crystal was harvested and cryoprotected by briefly soaking in a solution of the mother liquor with 20% of a 1:1 ethylene glycol/glycerol mixture added and flash cooled in the nitrogen stream at the MX-1 beamline of the Australian Synchrotron. One hundred eighty-one frames of 1° oscillations were collected, each frame being exposed for 8 seconds. The structure was solved using the molecular replacement program Phaser (31) and a previously determined antibody structure [Protein Data Bank (PDB) code 1IGF]. A known IGF-II structure was parsed out from another PDB file, 2V5P, and subsequently placed in the clear density for this part of the complex. The model was manually rebuilt using the program Coot (32), and the complex was refined using Refmac from the CCP4 package (31) using data to 2.4 Å. We subsequently collected higher-resolution data to 2.2 Å, and the structure was further refined. The crystallographic statistics are presented in the Supplementary Table.

In vitro phosphorylation studies using transfected cells

R-IGF-IR or R-IR-A cells [3T3-like mouse fibroblasts derived from the IGF-IR knockout mouse (17) transfected with human cDNA to express either IGF-IR or IR-A, respectively] were plated in 96-well flat-bottom plates (12×10^3 per well) and grown overnight at 37°C and 5% CO_2. Cells were washed twice in serum-free DMEM before being serum starved for 5 hours. Cells were then treated with dilutions of DX-2647 (or isotype control IgG) in either 3 or 30 nmol/L IGF-II/0.5% (w/v) bovine serum albumin (BSA)/DMEM for 10 minutes at 37°C and 5% CO_2. Cell lysates were then prepared, and receptor tyrosine phosphorylation was quantified using a europium-labeled anti-phosphotyrosine monoclonal antibody as described (27).

In vitro phosphorylation studies using select cancer cell lines

Cells were seeded into 60-mm dishes (1×10^6 per dish) in complete medium. After 24 hours of incubation, cells were serum starved in 5 mL of basal medium overnight and then treated with IGF-I, IGF-II, and DX-2647 or control IgG for 20 minutes at the indicated concentrations. Cells were washed thrice with ice-cold PBS containing 1 mmol/L Na_3VO_4 and then lysed with 1 mL of radioimmunoprecipitation assay buffer containing protease inhibitor cocktail. The lysates were centrifuged at 14,000 rpm for 10 minutes to remove cell debris. Equal amounts of proteins from each sample were immunoprecipitated with anti–IGF-IR antibody (2 μg per sample; Millipore) and protein G beads (40 μL per sample) and gently mixed overnight at 4°C. After washing thrice with 1 mL of radioimmunoprecipitation assay buffer, the beads were resuspended in 12 μL of 2× electrophoresis sample buffer and heated at 95°C for 5 minutes. Proteins were resolved in 4% to 12% Bis-Tris gels and then transferred to 0.45-μm polyvinylidene difluoride membranes. The blots were blocked with 5% (w/v) BSA-PBST [0.05% (v/v) Tween 20] for 1 hour, probed with rabbit anti–phospho-IGF-IR β (Try1131) antibody [1:1,000 diluted in 3% (w/v) BSA-PBST; Cell Signaling], followed by horseradish peroxidase–conjugated anti-rabbit IgG [1:5,000 diluted in 3% (w/v) BSA-PBST], and visualized with SuperSignal West Femto Maximum Sensitivity Substrate (Pierce). Blots were stripped with blot stripping buffer (Pierce) at 50°C for 30 minutes and then reprobed for total IGF-IR with 1:1,000 diluted anti–IGF-IR antibody. For the detection of phospho-IGF-IR mediated by endogenously produced IGF-II, cells were seeded into 60-mm dishes at a density of 1×10^6 per dish in complete medium. After 24 hours of incubation, cells were serum starved in 5 mL of basal medium containing DX-2647 at the indicated concentrations and for various times. Cell extracts were prepared and analyzed as described above.

Anchorage-independent colony formation assay

HepG2 cells (3×10^3 to 10×10^3) were resuspended in 1 mL of culture medium containing 10% FBS, 0.4% (w/v) low-melting-temperature agarose, and DX-2647 at various concentrations. The cell suspension was laid on top of 1.5 mL of 0.8% (w/v) agarose-containing medium in a six-well plate with 1 mL medium containing DX-2647 on top and placed in a 37°C incubator with 5% CO_2 for 2 weeks to allow colonies to form. Colonies (>50 cells) were scored in three independent experiments, each with triplicate dishes.

Anchorage-dependent colony formation assay

Hep3B cells (5×10^2 to 10×10^2) were seeded into six-well plates in culture medium containing 10% FBS and DX-2647 at various concentrations and placed in a 37°C incubator with 5% CO_2 for 1 week to allow colonies to form. Colonies (>50 cells) were scored in three independent experiments, each with triplicate dishes.

Hep3B xenograft model

Each mouse was inoculated s.c. at the right flank with the Hep3B tumor cells (5×10^6) in 0.1 mL PBS with Matrigel (1:1) for tumor development. The treatments were started on day 14 after tumor inoculation

Published OnlineFirst June 1, 2010; DOI: 10.1158/1535-7163.MCT-09-1134

when the tumor size reached ~100 mm^3. Each group consisted of nine tumor-bearing mice. All the procedures related to animal handling, care, and the treatment in this study were done according to guidelines approved by the Institutional Animal Care and Use Committee of Crown Bioscience (Beijing, China) following the guidance of the Association for Assessment and Accreditation of Laboratory Animal Care. Tumor size was measured twice weekly in two dimensions using a caliper, and the volume was expressed in mm^3 using the following formula: $V = 0.536\ a \times b^2$, where a and b are the long and short diameters of the tumor, respectively. Tumor weights were measured at study termination. Statistical analysis of difference in mean tumor volumes among the groups and the analysis of drug interaction were conducted on the data obtained. A one-way ANOVA was done, and when a significant F statistics (a ratio of treatment variance to the error variance) was obtained, comparisons between groups were carried out with a least significant difference test. All data were analyzed using SPSS 17.0. $P < 0.05$ was considered to be statistically significant.

Immunohistochemical analyses

Primary tumors were removed, processed, and subjected to immunohistochemical analysis. All the stainings were done on paraffin sections (4 μm). Slides were treated with Target Retrieval Solution, low pH (DakoCytomation) at 100°C for 20 minutes; endogenous peroxidase activity and nonspecific binding sites were blocked with Peroxidase Block (DakoCytomation) and Protein Block Serum Free (DakoCytomation) separately, and primary antibodies were incubated overnight at 4°C. The detection systems used were either EnVision+ System-HPR (DakoCytomation) or Alexa Fluor 488 goat anti-human (1:200; Invitrogen), or Alexa Fluor 594 goat anti-rabbit secondary antibodies (1:200; Invitrogen). 3,3′-Diaminobenzidine (DakoCytomation) was used as a chromogen, and the slides were counterstained with hematoxylin (DakoCytomation) for immunohistochemical staining and with 4′,6-diamidino-2-phenylindole (1 μg/mL; Invitrogen) for immunofluorescence staining.

Primary antibodies used for this study were from the following sources: polyclonal rabbit anti-human IgG (1:100; DakoCytomation), monoclonal mouse anti-human Ki67 antigen (1:150; DakoCytomation), polyclonal rabbit anti-mouse PECAM (CD31; 1:100; Santa Cruz Biotechnology), polyclonal rabbit anti-human IGF-IIE (1:150; Novozymes GroPep), goat anti-human IGF-II (5 μg/mL; R&D Systems), goat anti-human IGF-I (5 μg/mL; R&D Systems), polyclonal rabbit anti–IGF-IR (5 μg/mL; GenScript), and polyclonal rabbit anti–IGF-IR (phospho-Tyr^{1161}; 5 μg/mL; GenScript). Terminal deoxynucleotidyl transferase–mediated dUTP nick end labeling (TUNEL) assay was done with the TUNEL Apoptosis Detection kit (GenScript) according to the manufacturer's protocol.

Results

Selections and screening

A human Fab-on-phage display library was screened with biotinylated IGF-IIE (1–104 amino acids; refs. 29, 33). More than 200 individual clones were isolated and subsequently characterized for specificity (IGF-II versus IGF-IIE), affinity, and ability to block ligand-induced cell proliferation. Ba/F3 cells are an IL-3–dependent murine pro-B-cell line established from peripheral blood derived from a BALB/c mouse in which IL-4 synergizes with IGF-I in stimulating proliferation in an IL-3–independent manner (28). To determine if this cell line could be used for high-throughput screening of anti–IGF-II/IGF-IIE soluble Fabs (sFab), we first showed that IL-4 also synergized with IGF-II or IGF-IIE in stimulating cell proliferation (Fig. 1A). High levels (2,000 endotoxin units/mL) of lipopolysaccharide showed no significant effect on cell proliferation (Fig. 1A), thus allowing us to screen for bioactivity of *Escherichia coli*–expressed sFabs. Two batches (total of 41 sFabs) were screened in the Ba/F3 proliferation

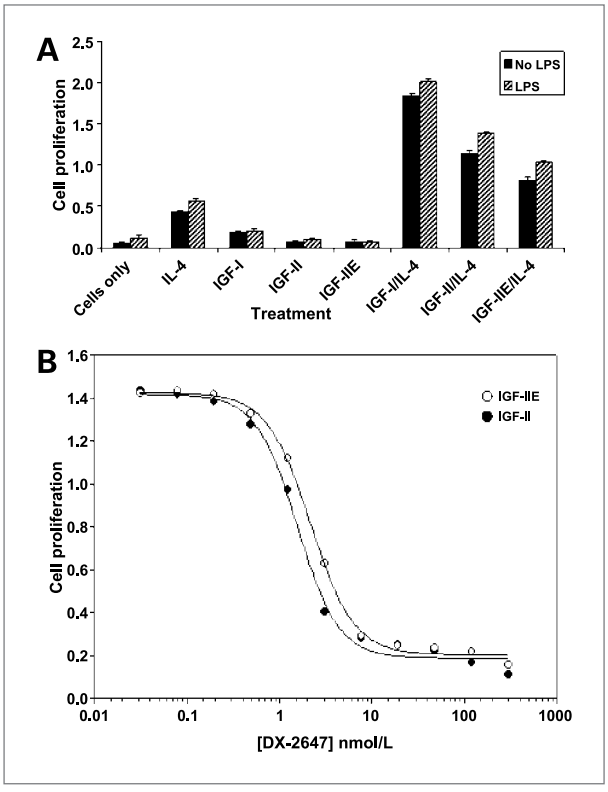

Figure 1. DX-2647 blocks IGF-II–stimulated proliferation. A, IGF-II/IGF-IIE synergizes with IL-4 to stimulate Ba/F3 cell proliferation. Ba/F3 cells were stimulated with the indicated cytokines, growth factors, or combinations thereof in the presence or absence of lipopolysaccharide (LPS). Proliferation was assessed after 2 d. B, representative plot of DX-2647–induced inhibition of IGF-II–stimulated and IGF-IIE (100 ng/mL)–stimulated Ba/F3 cell proliferation. $n = 3$ for each experiment.

Published OnlineFirst June 1, 2010; DOI: 10.1158/1535-7163.MCT-09-1134

assay, and the most potent of these Fabs was further codon optimized, germlined, reformatted into IgG1, expressed, and purified. One of these antibody leads (DX-2647) was retested in the Ba/F3 cell proliferation assay and showed a potent dose-dependent inhibition of both IGF-II– and IGF-IIE–induced proliferation (Fig. 1B).

Analytic biochemistry

The affinity of DX-2647 to recombinant isoforms of IGF-II and IGF-IIE was determined using SPR with the IgG "captured" onto an anti-human Fc Ig-coupled chip, followed by injection of ligand analyte. Affinity measurements revealed that DX-2647 bound both IGF-II and IGF-IIE with very high affinity (K_D values of 49 and 10 pmol/L, respectively; Fig. 2A). Although IGF-II and the related growth factor, IGF-I, share 70% homology at the amino acid level, SPR results showed that DX-2647 bound IGF-I with a K_D value significantly weaker (9.6 nmol/L) than that for IGF-II/IGF-IIE (Fig. 2A).

Although IGF-IR and IR-A are the principal mediators of IGF-II bioactivity, the protein can bind with high affinity to a number of other proteins that include a family of six serum IGFBPs (IGFBP-1 to IGFBP-6) and the cell surface mannose-6-phosphate receptor (IGF-IIR). A number of different assay formats using SPR were used to assess whether DX-2647 could still bind IGF-II or IGF-IIE when complexed with other proteins or vice versa. Fc-captured human antibody binds free IGF-II but does not bind a preformed complex of IGF-II and IGFBP-1 or IGFBP-1 alone (Fig. 2B). Although DX-2647 blocks the binding of both IGF-II and IGF-IIE to all three cell surface receptors for IGF-II, its ability to bind both ligands complexed with IGFBPs is inhibited (Fig. 2B, inset table). This latter observation may be beneficial with respect to the pharmacokinetic profile of DX-2647 *in vivo*.

Structural studies

To better characterize the potential ligand sequestering ability of DX-2647, we resolved the crystal complex of IGF-II in complex with M0064-F02, the parental, nongermlined Fab from which DX-2647 was derived. The cocrystal complex was solved to 2.2 Å resolution, and a ribbon representation of the complex between IGF-II (red) and Fab M0064-F02 is shown (Fig. 2C). The Fab heavy chain (green) makes a number of contacts with the first α-helix of the IGF-II A domain, whereas residues from CDR3 extend into a hydrophobic pocket formed by the ligand. Interactions are observed between residues on the light chain (yellow) and the first turn of the B domain α-helix. The combined contact surface area on IGF-II is 849 $Å^2$ and encompasses key residues in IGF-II that have been identified by mutagenesis as being critical for binding to both IGF-IR and IR, and the IGFBPs (data not shown). The complex can be superposed with the recently reported IGF-IIR–IGF-II complex structure (34). Forty-five of the 48 residues of IGF-II in common could be aligned (residues 30–39 of IGF-II are missing in the receptor complex structure) and were superposed with a root mean square deviation of 1.4 Å. There are some large differences in the two IGF-II structures near the missing loop, with residues Tyr^{27} through Ile^{42} being outside a 1.5 Å radius of convergence. This loop is not involved in the binding of IGF-II to the IGF-IIR but is peripherally involved in binding to the Fab (Fig. 2D). Analyzing the superposed structures reveals that there is little overlap in the two binding domains (Fab versus IGF-IIR), except around the loop Gln^{1569} to Arg^{1571} of the receptor, which competes with Ser^{31} and Tyr^{93} of the light chain for space around Asp^{15} of IGF-II.

Cell signaling studies

On ligand binding, the two β-subunits of IGF-IR and IR-A undergo autophosphorylation on tyrosine residues. We sought to assess whether DX-2647 could block IGF-II–induced IGF-IR and IR-A phosphorylation. Using transfected mouse 3T3 cells expressing either human IR-A or IGF-IR, we showed that DX-2647 dose dependently inhibited IGF-II–induced phosphorylation of each receptor (Fig. 3A and B). In addition, we also showed that DX-2647 was able to efficiently block, in a dose-dependent manner, IGF-II–induced (exogenously added) IGF-IR phosphorylation in Colo205, HepG2, and Hep3B cells (Fig. 3C). DX-2647 binds to IGF-I at much lower affinity compared with binding to IGF-II based on SPR analysis. Consequently, DX-2647 showed only a very slight inhibition of IGF-I–induced IGF-IR phosphorylation in Hep3B cells (Fig. 3C). Thus, higher concentrations of DX-2647 may be required to obtain an inhibitory effect against IGF-I. Hep3B cells synthesize and secrete IGF-II, which in turn binds IGF-IR and induces IGF-IR phosphorylation in an autocrine fashion. This autocrine stimulatory loop can be detected by immunoprecipitation/Western blot analysis after 48 hours of serum starvation of cells. DX-2647 at 10 nmol/L showed significant inhibitory effect on autocrine IGF-II–induced IGF-IR phosphorylation in Hep3B cells (Fig. 3C, bottom right). Similar results were obtained with a 24-hour treatment of DX-2647 (data not shown).

Anchorage-independent and anchorage-dependent growth of hepatocellular cancer cell lines

To further characterize the *in vitro* effects of DX-2647, we did a series of cell-based colony formation assays. Using both HepG2 and Hep3B cells, we showed that DX-2647 inhibited both anchorage-independent (HepG2) and anchorage-dependent (Hep3B) growth of colonies in a dose-dependent manner (Fig. 4A and B). These data suggest that sequestration of IGF-II and subsequent inhibition of downstream signaling events in these cell types are sufficient to retard growth of both these cell lines.

DX-2647 inhibits Hep3B xenograft tumor progression

The therapeutic efficacy of DX-2647 on the Hep3B human HCC xenograft model was evaluated. Animals were treated with DX-2647, pegvisomant (human growth

Published OnlineFirst June 1, 2010; DOI: 10.1158/1535-7163.MCT-09-1134

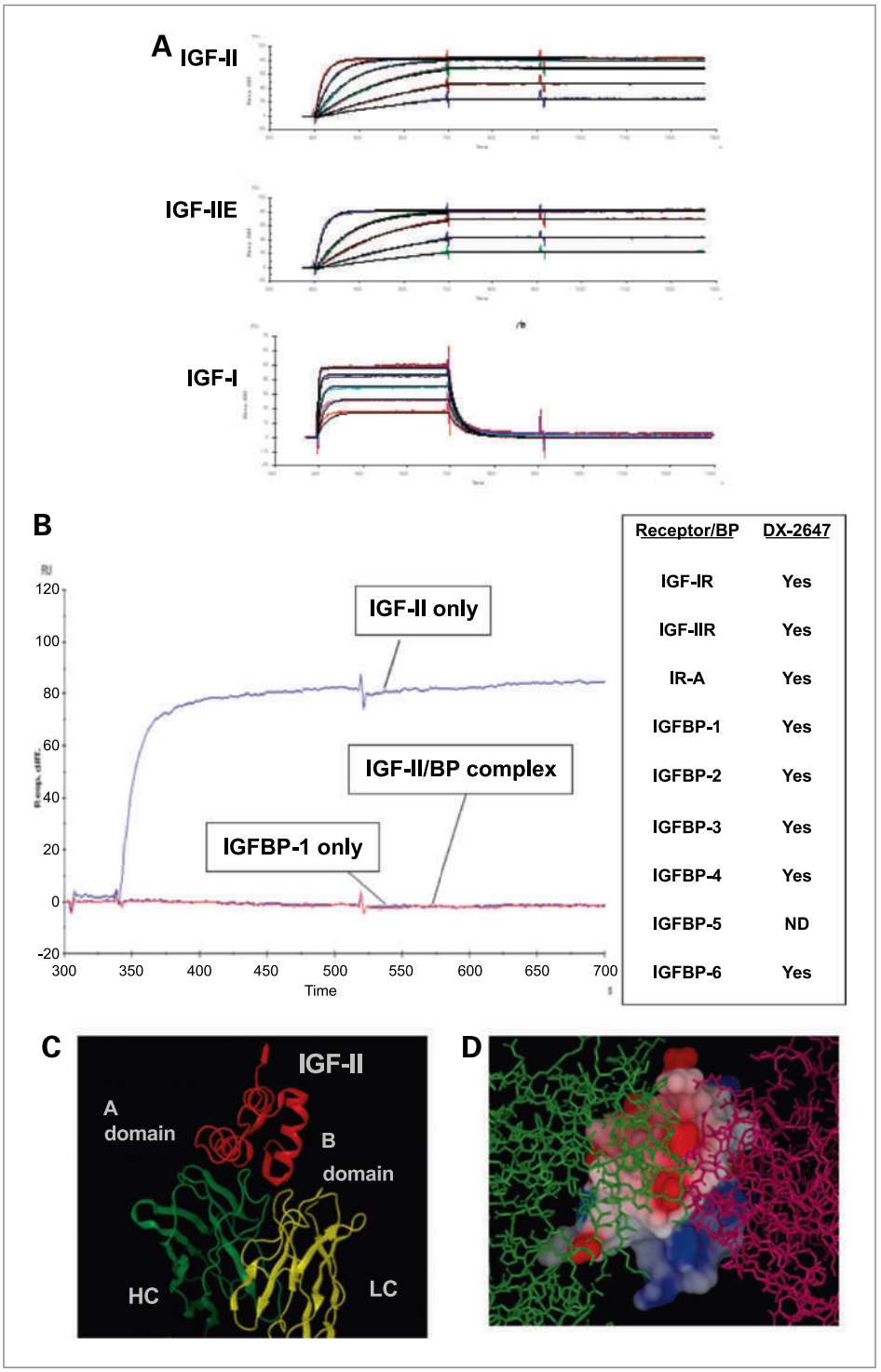

Figure 2. DX-2647 binds to IGF-II with high affinity. A, kinetic analysis of IGF-II, IGF-IIE, and IGF-I binding to DX-2647. Mean values and SDs for the kinetic parameters k_a and k_d were determined from n independent experiments as $1.8 \pm 0.7 \times 10^6$ mol/L^{-1} s^{-1} and $8.9 \pm 4.8 \times 10^{-5}$ s^{-1} for IGF-II ($n = 4$), $1.9 \pm 1.3 \times 10^6$ mol/L^{-1} s^{-1} and 2.0 ± 1.0 10^{-5} s^{-1} for IGF-IIE ($n = 4$), and $2.5 \pm 0.9 \times 10^6$ mol/L^{-1} s^{-1} and 2.4 ± 0.4 10^{-2} s^{-1} for IGF-I. Average K_D values for IGF-II, IGF-IIE, and IGF-I were calculated as 49.4 pmol/L, 10.5 pmol/L, and 9.6 nmol/L, respectively. B, representative SPR tracing and tabular data showing that DX-2647 does not bind to precomplexed IGF-II. C, a ribbon representation of the crystal complex of the parental Fab of DX-2647 and IGF-II. IGF-II is shown in red at the top of the figure, with the heavy and light chains of the Fab shown in green and yellow, respectively. D, molecular surface representation of IGF-II (colored by electrostatic potential) with the Fab shown in a stick representation in burgundy (on the right) and the IGF-IIR structure also shown in stick representation in green (on the left; PDB code 2V5P). Both images (C and D) were generated with the program Afitt (OpenEye Scientific Software). The superposition of the IGF-II structures was done in Coot using the SSM algorithm (48).

hormone receptor antagonist), or PBS at the indicated dosages every other day for the duration of the study. DX-2647 produced a 60% slowing of tumor progression compared with the group receiving PBS alone (Fig. 5A). Interestingly, pegvisomant, known to decrease serum IGF-I levels in mice (35) and humans (36), had no significant effect on tumor progression in this model. The effect on tumor progression equated with an approximate tumor growth delay of 9 days in the group treated with DX-2647. In addition to the observed effects on tumor progression, tumor wet weight was significantly decreased (Fig. 5B). All treatments were tolerated well

Published OnlineFirst June 1, 2010; DOI: 10.1158/1535-7163.MCT-09-1134

by the tumor-bearing animals, with no severe body weight loss observed during the treatment period (Fig. 5C).

Morphologic and immunohistochemical analysis of Hep3B tumors

To assess tumor uptake of DX-2647, human IgG immunostaining was done on tumor sections from all treated groups. Positive staining was observed in tumors exposed to DX-2647 (Fig. 6A, a–c) and localized in specific areas: membrane and cytosol of tumor cells, endothelium of blood vessels (Fig. 6A, c1–c3), and connective tissues around tumor cells (data not shown). This reflected the high exposure of Hep3B tumors to DX-2647. Consistent with this, circulating levels of DX-2647 reached ~80 μg/mL, further confirming significant exposure in these animals (data not shown).

Histologically, Hep3B tumor cells were arranged as nests separated by bundles of extracellular matrix (Fig. 6A, d–i, arrows), where blood vessels were localized. Some tumor nests had a central lumen filled with blood, which is similar to the central vein surrounded with trabecular structures, resembling normal liver plates (Fig. 6A, d–f). No lobule-like structures were identified in PBS control–treated and pegvisomant-treated samples in contrast to those obtained from DX-2647–treated animals (Fig. 6A, d–f).

We did additional immunohistochemical analyses to assess the possible mechanism(s) by which DX-2647 showed antitumor activity. TUNEL assay showed no difference in apoptosis among groups (Fig. 6A, j–l) in accordance with our histologic observations (Fig. 6A, g–i). No differences in Ki67 staining were observed (data not shown). Interestingly, DX-2647 treatment led to a significant reduction of tumor vascularization (as measured by a reduction in staining for the endothelial marker CD31), affecting both the number and the size of the vessels (Fig. 6A, m–o). This suggests that the antitumor activity of DX-2647 may be due to the inhibition of angiogenesis.

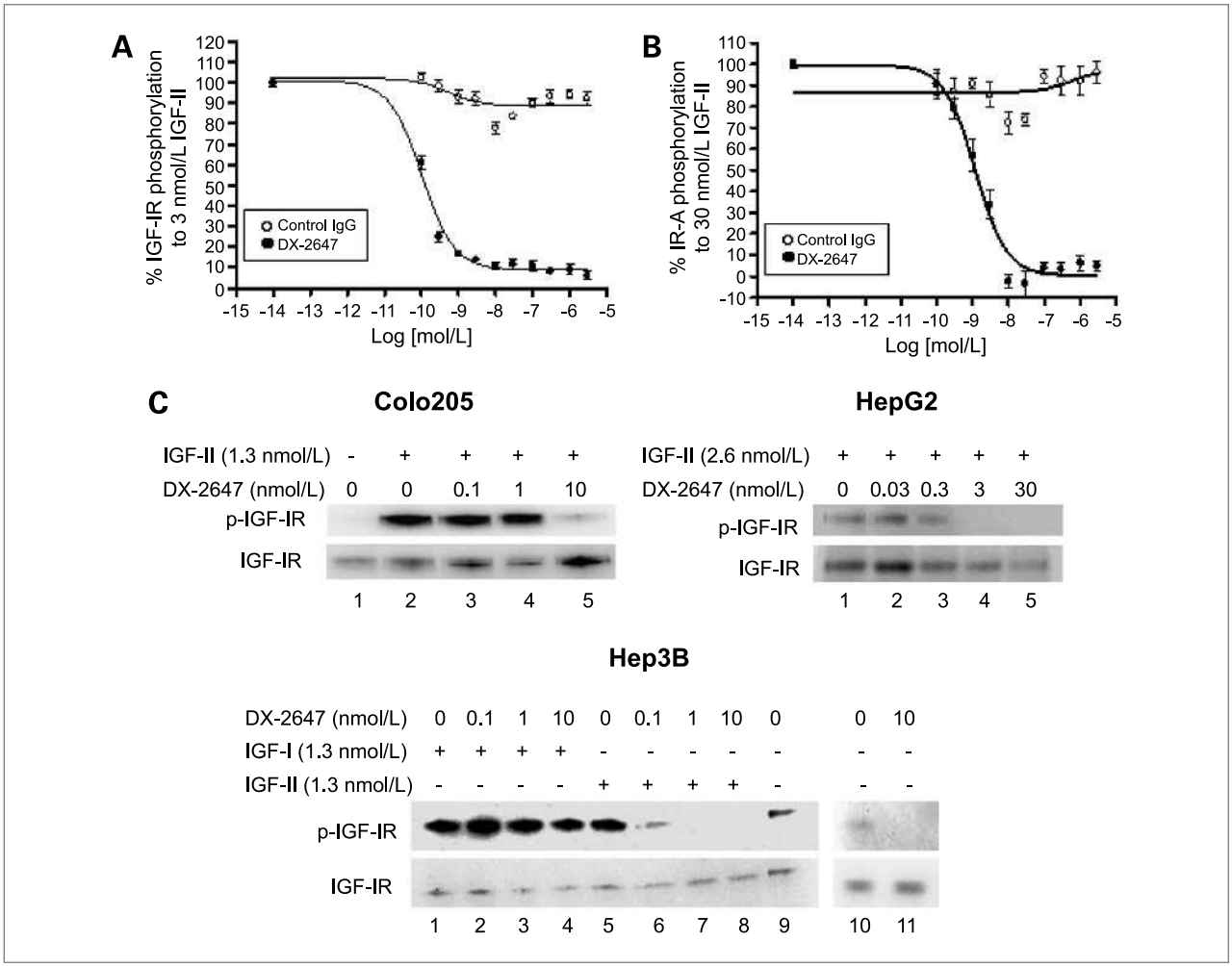

Figure 3. DX-2647 blocks IGF-driven cell signaling events. Dose-dependent inhibition of IGF-II stimulated phosphorylation of IGF-IR (A) or IR-A (B) in transfected NIH-3T3 cells. C, DX-2647 blocks exogenous and endogenous IGF-II/IGF-I–mediated phosphorylation of IGF-IR in select cancer cell lines. $n = 3$ for each experiment.

Published OnlineFirst June 1, 2010; DOI: 10.1158/1535-7163.MCT-09-1134

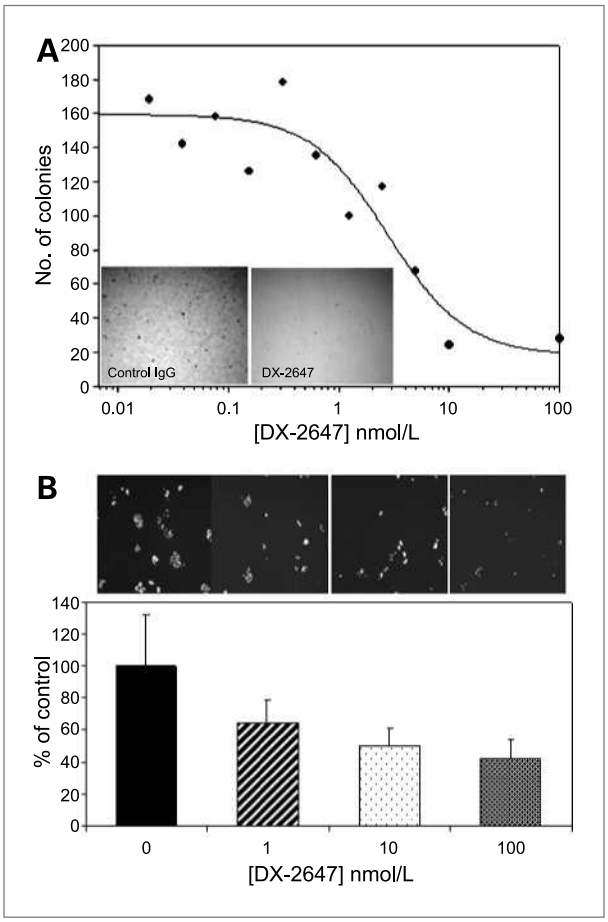

Figure 4. DX-2647 inhibits anchorage-independent and anchorage-dependent colony formation in HCC cell lines. A, HepG2 cell anchorage-independent colony formation. Representative images of colonies are shown (inset). B, Hep3B-cell anchorage-dependent colony formation. Representative images for each respective dose of DX-2647 tested are shown above each bar. $n = 3$ for each experiment.

We next analyzed the tumoral expression level of different components of the IGF pathway. Our immunohistochemical analysis showed a downregulation of IGF-IIE and phospho-IGF-IR levels in tumors from DX-2647–treated animals and a downregulation of IGF-I expression in the pegvisomant-treated group (Fig. 6B).

Discussion

The overexpression of IGF-II by a variety of human cancer types including HCC, together with the ability of this growth factor to use at least two receptors (IGF-IR and IR-A) to drive tumor cell proliferation, suggests that targeting this growth factor directly has potential as a therapeutic option. Using our phage display technologies, we have identified a fully human antibody, DX-2647, which binds with high potency and selectivity toward IGF-II/IGF-IIE and significantly inhibits the growth of tumor xenografts derived from the human HCC cell line Hep3B.

Phage-derived human monoclonal antibodies binding both IGF-II and IGF-IIE (pro-IGF-II) with high affinity (~1 nmol/L) have been previously described (25, 26). These antibodies did not cross-react with IGF-I or insulin and inhibited IGF-II–induced receptor phosphorylation (both IGF-IR and IR), cellular proliferation and motility, and *in vivo* growth of prostate cancer cells in a human

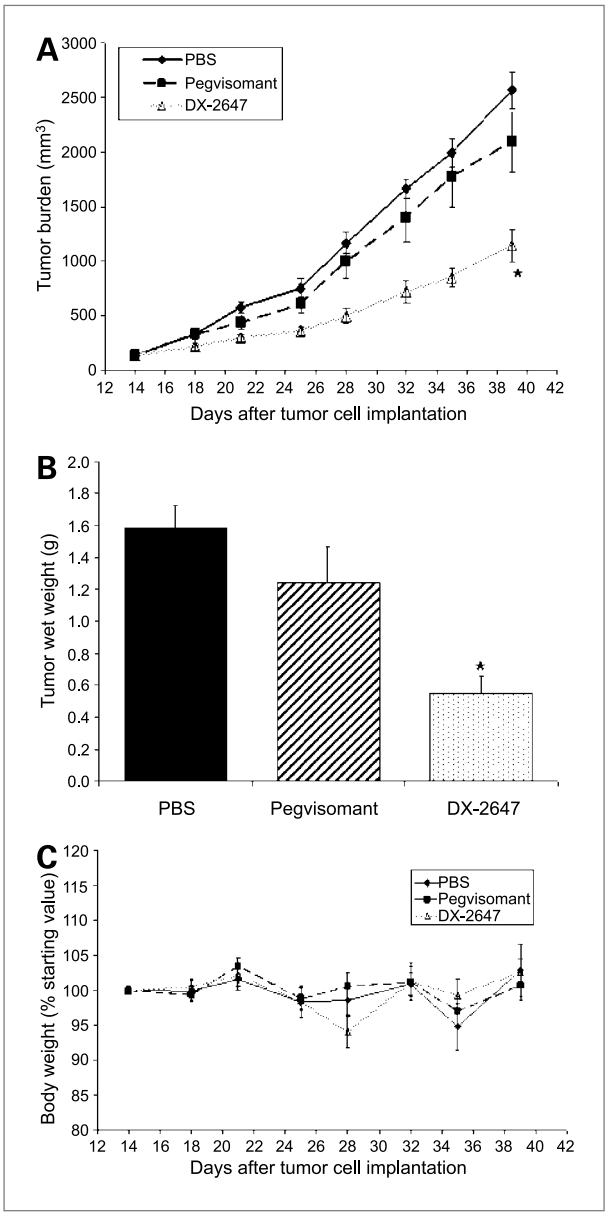

Figure 5. DX-2647 slows tumor progression in the Hep3B hepatocellular xenograft model. A, tumor burden graph depicting slowing of tumor progression by DX-2647. B, tumor wet weight after tumor excision (day 39). C, animal body weight over time indicates no significant changes due to treatment regimen. Number of animals for each group is eight to nine. *, $P < 0.05$, compared with PBS-treated control group.

Published OnlineFirst June 1, 2010; DOI: 10.1158/1535-7163.MCT-09-1134

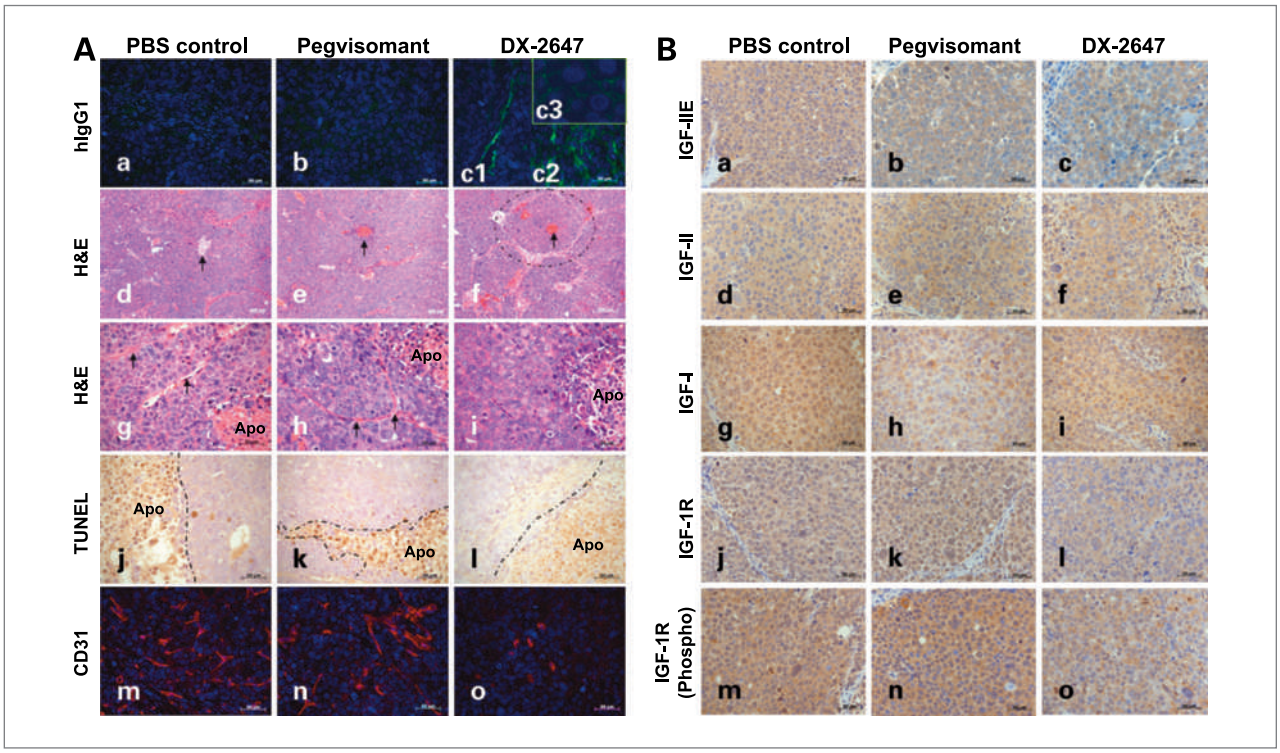

Figure 6. Immunohistochemical analysis of tumors from DX-2647–treated animals reveals decreased CD31 staining and reduced levels of IGF-IIE and IGF-IR phosphorylation levels. A, H&E and immunohistochemical evaluation of human xenograft Hep3B tumors. Tumor sections were stained with H&E and immunohistochemistry for human IgG1 (hIgG1), TUNEL assay (brown), and CD31 (red) as described in Materials and Methods. Pictures are representative of four animals from each group. Apo, apoptosis. Dotted line delineates apoptotic areas. Magnifications, ×400 (a, b, c1–c3, and g–o) and ×100 (d–f). B, immunohistochemical evaluation IGF pathway molecules. Tumor sections were stained for IGF-IIE, IGF-II, IGF-I, IGF-IR, and IGF-IR-phospho as described in Materials and Methods. Pictures are representative of four animals from each group. Magnification, ×400.

bone environment. By comparison, DX-2647 bound IGF-II/IGF-IIE with very high affinity but also cross-reacted with IGF-I, albeit with much lower affinity (K_D, ~10 nmol/L). The antibody potently inhibited IGF-II–induced receptor activation in transfected mouse fibroblasts and human colorectal and HCC cell lines. In cell-based studies, DX-2647 blocked IGF-II– and IGF-IIE–mediated proliferation of Ba/F3 cells and suppressed the anchorage-dependent (Hep3B) and anchorage-independent (HepG2) growth of human HCC cell lines. HCC cell lines have been shown to secrete significant amounts of IGF-II, which not only provides an autocrine growth stimulus but also inhibits apoptosis induced by chemotherapeutic agents (37). The protumorigenic activity of IGF-II in Hep3B and another human HCC cell line, HuH7, was shown to be solely transmitted via IGF-IR, with little evidence for a role for IGF-I (38). From a pharmacokinetic perspective, the inability of DX-2647 to bind to IGF-II/IGF-IIE when complexed with IGFBPs would seem to be a beneficial characteristic for *in vivo* use, given the high circulating levels of IGF-II/IGFBP complexes in normal serum (20, 21). The resolution of the crystal complex of the parental Fab and IGF-II has confirmed a structural basis for this. In the example provided for comparison, that of IGF-IIR in complex with IGF-II (34), the small overlap of Fab and IGF-IIR observed following supposition of IGF-II is clearly sufficient to sterically block both proteins, binding to IGF-II simultaneously, and includes a key residue, Thr^{1570}, on the IGF-IIR that is required for IGF-II binding (39).

The sensitivity of Hep3B xenografts to IGF-II blockade is perhaps not surprising. Orthotopic tumors derived following injection of Hep3B into the liver parenchyma of nude mice overexpressed IGF-II mRNA and protein, whereas inhibition of IGF-II mRNA using an antisense oligonucleotide significantly prolonged animal survival (40, 41). There was no analysis of tumor biomarkers to identify the consequences of such treatment. Although markers of tumor proliferation (Ki67 staining) and apoptosis (TUNEL) were qualitatively similar in tumor tissue from control and DX-2647–treated animals, there was a marked decline in CD31 staining following DX-2647 treatment, suggesting an antiangiogenic property of this antibody. HCC is regarded as a hypervascular tumor; treatment of HepG2 cells with IGF-II induces vascular endothelial growth factor expression, a response augmented by hypoxia (42). IGF-II stimulates chemotaxis and morphologic differentiation of human umbilical vascular endothelial cells into a capillary network (43) and promotes the outgrowth of CD31-positive endothelial cells from

Published OnlineFirst June 1, 2010; DOI: 10.1158/1535-7163.MCT-09-1134

hemangioma explants (44). In an intriguing twist, it may be that at least some of the angiogenic activity elicited by IGF-II is mediated through another receptor, IGF-IIR, which plays a key role in regulating the bioavailability of IGF-II (4). A mutant form of IGF-II that could not bind IGF-IR but retained the ability to bind IGF-IIR stimulated endothelial cell migration and neovascularization (45), whereas IGF-II promoted the homing of endothelial progenitor cells and enhanced angiogenesis *in vivo*, largely via IGF-IIR (46). Therefore, the antiangiogenic effects of DX-2647 we observed could be mediated in part by its ability to block IGF-II/IGF-IIE–mediated angiogenic activity in the Hep3B tumors. We are actively assessing further the antiangiogenic properties of DX-2647.

Immunohistochemical analysis revealed a marked decline in IGF-IIE levels in the tumors from DX-2647–treated animals and a concomitant decline in IGF-IR phosphorylation levels. Effects on IR-A phosphorylation status were not determined, as suitable reagents to assess this signaling event in tumor tissues do not exist. Why there is a selective effect of DX-2647 on tumor IGF-IIE and not IGF-II is unknown at this time. So-called big IGF-II isoforms isolated from the tumor tissue of two patients, corresponding to partially processed pro-IGF-II, retained the ability to form binary complexes with IGFBP-1 to IGFBP-6 but impaired the formation of the ternary complex with acid labile subunit when bound to IGFBP-3 (47). Even so, DX-2647 cannot bind either IGF-II or IGF-IIE when the growth factor exists in a binary complex with the five IGFBPs assayed (Fig. 2B). On the other hand, noncomplexed, tumor-associated pro-IGF-II isoforms are secreted by a number of soft tissue sarcoma cell lines (7). The biochemical nature of IGF-II secreted by Hep3B cells has not been characterized to our knowledge. Our results infer that *in vivo*, Hep3B xenografts secrete a bioavailable form of IGF-IIE, the antibody-mediated sequestration of which is accompanied by a reduction in IGF-IR activation, inhibition of angiogenesis (involving IGF-IIR?), and retardation of tumor growth.

Although targeting agents toward IGF-IR can block IGF-I and IGF-II signaling through the receptor, this therapeutic approach is unable to block IGF-II– and IGF-IIE–mediated signaling through IR-A or, indeed, IGF-IIR. DX-2647 provides a therapeutic alternative to IGF-IR–targeted agents, which would serve to ablate IGF-II–driven tumor growth in a select number of cancers.

Disclosure of Potential Conflicts of Interest

D.T. Dransfield, E.H. Cohen, Q. Chang, N. Kastrapeli, K. Kopacz, D. Martik, D. Wassaf, D. Rank, G. Conley, and Y. Huang: employees, Dyax Corp. D.T. Dransfield, E.H. Cohen, T.E. Adams, and L. Cosgrove have submitted patent applications stemming from this work and are listed as inventors. No other potential conflicts of interest were disclosed.

Acknowledgments

We thank the beamline scientists at the Australian Synchrotron for their help with data collection.

The costs of publication of this article were defrayed in part by the payment of page charges. This article must therefore be hereby marked *advertisement* in accordance with 18 U.S.C. Section 1734 solely to indicate this fact.

Received 12/08/2009; revised 03/12/2010; accepted 04/18/2010; published OnlineFirst 06/01/2010.

References

1. El-Serag HB, Rudolph KL. Hepatocellular carcinoma: epidemiology and molecular carcinogenesis. Gastroenterology 2007;132:2557–76.
2. Spangenberg HC, Thimme R, Blum HE. Evolving therapies in the treatment of hepatocellular carcinoma. Biologics 2008;2:453–62.
3. Breuhahn K, Schirmacher P. Reactivation of the insulin-like growth factor-II signaling pathway in human hepatocellular carcinoma. World J Gastroenterol 2008;14:1690–8.
4. Chao W, D'Amore PA. IGF2: epigenetic regulation and role in development and disease. Cytokine Growth Factor Rev 2008;19:111–20.
5. Duguay SJ, Jin Y, Stein J, Duguay AN, Gardner P, Steiner DF. Post-translational processing of the insulin-like growth factor-2 precursor. Analysis of *O*-glycosylation and endoproteolysis. J Biol Chem 1998; 273:18443–51.
6. Daughaday WH, Emanuele MA, Brooks MH, Barbato AL, Kapadia M, Rotwein P. Synthesis and secretion of insulin-like growth factor II by a leiomyosarcoma with associated hypoglycemia. N Engl J Med 1988;319:1434–40.
7. Elmlinger MW, Rauschnabel U, Koscielniak E, Weber K, Ranke MB. Secretion of noncomplexed 'Big' (10-18 kD) forms of insulin-like growth factor-II by 12 soft tissue sarcoma cell lines. Horm Res 1999;52:178–85.
8. Ng IO, Lee JM, Srivastava G, Ng M. Expression of insulin-like growth factor II mRNA in hepatocellular carcinoma. J Gastroenterol Hepatol 1998;13:152–7.
9. Uchida K, Kondo M, Takeda S, et al. Altered transcriptional regulation of the insulin-like growth factor 2 gene in human hepatocellular carcinoma. Mol Carcinog 1997;18:193–8.
10. Cariani E, Lasserre C, Seurin D, et al. Differential expression of insulin-like growth factor II mRNA in human primary liver cancers, benign liver tumors, and liver cirrhosis. Cancer Res 1988;48:6844–9.
11. Park BC, Huh MH, Seo JH. Differential expression of transforming growth factor α and insulin-like growth factor II in chronic active hepatitis B, cirrhosis and hepatocellular carcinoma. J Hepatol 1995;22: 286–94.
12. Dong ZZ, Yao DF, Yao DB, et al. Expression and alteration of insulin-like growth factor II-messenger RNA in hepatoma tissues and peripheral blood of patients with hepatocellular carcinoma. World J Gastroenterol 2005;11:4655–60.
13. Rogler CE, Yang D, Rossetti L, et al. Altered body composition and increased frequency of diverse malignancies in insulin-like growth factor-II transgenic mice. J Biol Chem 1994;269:13779–84.
14. Cariani E, Dubois N, Lasserre C, Briand P, Brechot C. Insulin-like growth factor II (IGF-II) mRNA expression during hepatocarcinogenesis in transgenic mice. J Hepatol 1991;13:220–6.
15. Schirmacher P, Held WA, Yang D, Chisari FV, Rustum Y, Rogler CE. Reactivation of insulin-like growth factor II during hepatocarcinogenesis in transgenic mice suggests a role in malignant growth. Cancer Res 1992;52:2549–56.
16. Baserga R, Peruzzi F, Reiss K. The IGF-1 receptor in cancer biology. Int J Cancer 2003;107:873–7.
17. Sell C, Dumenil G, Deveaud C, et al. Effect of a null mutation of the insulin-like growth factor I receptor gene on growth and transformation of mouse embryo fibroblasts. Mol Cell Biol 1994;14:3604–12.
18. Sell C, Rubini M, Rubin R, Liu JP, Efstratiadis A, Baserga R. Simian

Published OnlineFirst June 1, 2010; DOI: 10.1158/1535-7163.MCT-09-1134

virus 40 large tumor antigen is unable to transform mouse embryonic fibroblasts lacking type 1 insulin-like growth factor receptor. Proc Natl Acad Sci U S A 1993;90:11217–21.
19. Rodon J, DeSantos V, Ferry RJ, Jr., Kurzrock R. Early drug development of inhibitors of the insulin-like growth factor-I receptor pathway: lessons from the first clinical trials. Mol Cancer Ther 2008;7:2575–88.
20. Renehan AG, Jones J, O'Dwyer ST, Shalet SM. Determination of IGF-I, IGF-II, IGFBP-2, and IGFBP-3 levels in serum and plasma: comparisons using the Bland-Altman method. Growth Horm IGF Res 2003;13:341–6.
21. Jones JI, Clemmons DR. Insulin-like growth factors and their binding proteins: biological actions. Endocr Rev 1995;16:3–34.
22. Belfiore A, Frasca F, Pandini G, Sciacca L, Vigneri R. Insulin receptor isoforms and insulin receptor/insulin-like growth factor receptor hybrids in physiology and disease. Endocr Rev 2009;30:586–623.
23. Goya M, Miyamoto S, Nagai K, et al. Growth inhibition of human prostate cancer cells in human adult bone implanted into nonobese diabetic/severe combined immunodeficient mice by a ligand-specific antibody to human insulin-like growth factors. Cancer Res 2004;64:6252–8.
24. Miyamoto S, Nakamura M, Shitara K, et al. Blockade of paracrine supply of insulin-like growth factors using neutralizing antibodies suppresses the liver metastasis of human colorectal cancers. Clin Cancer Res 2005;11:3494–502.
25. Feng Y, Zhu Z, Xiao X, Choudhry V, Barrett JC, Dimitrov DS. Novel human monoclonal antibodies to insulin-like growth factor (IGF)-II that potently inhibit the IGF receptor type I signal transduction function. Mol Cancer Ther 2006;5:114–20.
26. Kimura T, Kuwata T, Ashimine S, et al. Targeting of bone-derived insulin-like growth factor-II by a human neutralizing antibody suppresses the growth of prostate cancer cells in a human bone environment. Clin Cancer Res 2010;16:121–29.
27. Denley A, Bonython ER, Booker GW, et al. Structural determinants for high-affinity binding of insulin-like growth factor II to insulin receptor (IR)-A, the exon 11 minus isoform of the IR. Mol Endocrinol 2004;18:2502–12.
28. Soon L, Flechner L, Gutkind JS, et al. Insulin-like growth factor I synergizes with interleukin 4 for hematopoietic cell proliferation independent of insulin receptor substrate expression. Mol Cell Biol 1999;19:3816–28.
29. Newman J, Cohen EH, Cosgrove L, et al. Crystallization and preliminary X-ray analysis of the complexes between a Fab and two forms of human insulin-like growth factor II. Acta Crystallogr Sect F Struct Biol Cryst Commun 2009;65:945–8.
30. Newman J. Novel buffer systems for macromolecular crystallization. Acta Crystallogr D Biol Crystallogr 2004;60:610–2.
31. Collaborative Computational Project, Number 4. The CCP4 suite: programs for protein crystallography. Acta Crystallogr D Biol Crystallogr 1994;50:760–3.
32. Emsley P, Cowtan K. Coot: model-building tools for molecular graphics. Acta Crystallogr D Biol Crystallogr 2004;60:2126–32.
33. Hoet RM, Cohen EH, Kent RB, et al. Generation of high-affinity human antibodies by combining donor-derived and synthetic complementarity-determining-region diversity. Nat Biotechnol 2005;23:344–8.
34. Brown J, Delaine C, Zaccheo OJ, et al. Structure and functional analysis of the IGF-II/IGF2R interaction. EMBO J 2008;27:265–76.
35. Divisova J, Kuiatse I, Lazard Z, et al. The growth hormone receptor antagonist pegvisomant blocks both mammary gland development and MCF-7 breast cancer xenograft growth. Breast Cancer Res Treat 2006;98:315–27.
36. Yin D, Vreeland F, Schaaf LJ, et al. Clinical pharmacodynamic effects of the growth hormone receptor antagonist pegvisomant: implications for cancer therapy. Clin Cancer Res 2007;13:1000–9.
37. Lund P, Schubert D, Niketeghad F, Schirmacher P. Autocrine inhibition of chemotherapy response in human liver tumor cells by insulin-like growth factor-II. Cancer Lett 2004;206:85–96.
38. Nussbaum T, Samarin J, Ehemann V, et al. Autocrine insulin-like growth factor-II stimulation of tumor cell migration is a progression step in human hepatocarcinogenesis. Hepatology 2008;48:146–56.
39. Zaccheo OJ, Prince SN, Miller DM, et al. Kinetics of insulin-like growth factor II (IGF-II) interaction with domain 11 of the human IGF-II/mannose 6-phosphate receptor: function of CD and AB loop solvent-exposed residues. J Mol Biol 2006;359:403–21.
40. Yao X, Hu JF, Daniels M, et al. A methylated oligonucleotide inhibits IGF2 expression and enhances survival in a model of hepatocellular carcinoma. J Clin Invest 2003;111:265–73.
41. Yao X, Hu JF, Daniels M, et al. A novel orthotopic tumor model to study growth factors and oncogenes in hepatocarcinogenesis. Clin Cancer Res 2003;9:2719–26.
42. Kim KW, Bae SK, Lee OH, Bae MH, Lee MJ, Park BC. Insulin-like growth factor II induced by hypoxia may contribute to angiogenesis of human hepatocellular carcinoma. Cancer Res 1998;58:348–51.
43. Lee OH, Bae SK, Bae MH, et al. Identification of angiogenic properties of insulin-like growth factor II in *in vitro* angiogenesis models. Br J Cancer 2000;82:385–91.
44. Ritter MR, Dorrell MI, Edmonds J, Friedlander SF, Friedlander M. Insulin-like growth factor 2 and potential regulators of hemangioma growth and involution identified by large-scale expression analysis. Proc Natl Acad Sci U S A 2002;99:7455–60.
45. Volpert O, Jackson D, Bouck N, Linzer DI. The insulin-like growth factor II/mannose 6-phosphate receptor is required for proliferin-induced angiogenesis. Endocrinology 1996;137:3871–6.
46. Maeng YS, Choi HJ, Kwon JY, et al. Endothelial progenitor cell homing: prominent role of the IGF2-IGF2R-PLCβ2 axis. Blood 2009;113:233–43.
47. Bond JJ, Meka S, Baxter RC. Binding characteristics of pro-insulin-like growth factor-II from cancer patients: binary and ternary complex formation with IGF binding proteins-1 to -6. J Endocrinol 2000;165:253–60.
48. Krissinel E, Henrick K. Secondary-structure matching (SSM), a new tool for fast protein structure alignment in three dimensions. Acta Crystallogr D Biol Crystallogr 2004;60:2256–68.

Published OnlineFirst June 1, 2010; DOI: 10.1158/1535-7163.MCT-09-1134

Molecular Cancer Therapeutics

A Human Monoclonal Antibody against Insulin-Like Growth Factor-II Blocks the Growth of Human Hepatocellular Carcinoma Cell Lines *In vitro* and *In vivo*

Daniel T. Dransfield, Edward H. Cohen, Qing Chang, et al.

Mol Cancer Ther 2010;9:1809-1819. Published OnlineFirst June 1, 2010.